Molinero-Fernández, A. et al. (2020) 'Polymer-Based Micromotor Fluorescence Immunoassay for On-the-Move Sensitive Procalcitonin Determination in Very Low Birth Weight Infants' Plasma', ACS sensors, 5(5), pp. 1336–1344.

Available at https://doi.org/10.1021/acssensors.9b02515

Polymer-based micromotors fluorescence immunoassay for *on-the-move* sensitive procalcitonin determination in very low birth weight infants' plasma.

Molinero-Fernández, Á. Moreno-Guzmán, M. Arruza, L. López, M. Á. Escarpa, A.

ACS Sens. **2020**, 5(5), 1336.

Abstract

A new fluorescence micromotor-based immunoassay (FMIm) has been developed for procalcitonin (PCT) determination as an early sepsis diagnostic analytical tool. The micromotors combine the high binding capacity of the specific antibodies onto their polymeric polypyrrole outer layer (PPy layer), with their magnetic guidance (Ni layer) and self-propulsion by catalytic generation of oxygen bubbles (PtNPs inner layer) to actively recognize the PCT antigen. This FMIm allowed a sensitive (LOD = 0.07 ng/mL) and direct PCT determination in clinical samples from very low weight infants (VLBWI) with sepsis suspicion, using small volumes of sample (25 µL) volumes of sample (25 µL) in a clinically relevant range of concentrations (0.5−150 ng/mL). The good agreement between PCT levels obtained by our micromotor-based method and routine immunofluorescence hospital determination demonstrates the feasibility for the analysis in VLBWI samples and its potential as a *point-of-care* diagnostic tool for sepsis.

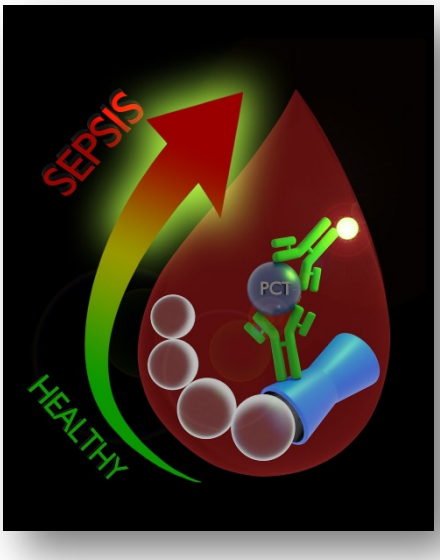

1. Introduction

Micromotors are microscale objects, which convert chemical energy or an external stimulus (chemical reaction, magnetic, ultrasound, or light) into autonomous propulsion.[1]

Considerable efforts have been devoted to chemically powered microscale motors based on surface catalytic decomposition of a fuel solution, usually hydrogen peroxide with oxygen bubble generation and subsequently propulsion. Template electrosynthesis has commonly been used because of the high versatility and low cost compared with rolled-up technology, which requires clean-room facilities and specialized personnel.[2,3]

These so-called bubble-propelled catalytic micromotors have demonstrated propulsion capabilities in high ionic strength media, opening the door for direct analytical measurements in complex biological or food samples.[4,5] The asset behind is the ability to move autonomously around the sample to actively find the specific analyte, together with the so-called fluid mixing effect producing a favorable hydrodynamic environment, which improves greatly the kinetics of the biorecognition interactions.[6−9]

This new micromotor-based paradigm in the biochemical assays paves the way for the development of new biosensing strategies of biomarkers. Several micromotors have been prepared by template-based electrodeposition of conductive polymers, which offer biofunctionalization capabilities.[2,10−13]

However, although their viability of biofunctionalization has been demonstrated, none of them have been evaluated to address an important clinical application, involving the analysis of real clinical samples. Therefore, it is necessary to begin exploring real biosensing applications of this type of micromotors.

Indeed, micromotor-based sensing diagnostic approaches are very interesting, especially in the clinical practice in situations where biological samples are hardly available. A relevant example is sepsis diagnosis in very low

birth weight infants (VLBWI) where the extraction of large volumes of samples is inadvisable.

Although there has been great improvement in antibiotic therapy and life support, the global death rate of adult and neonatal sepsis remains high.[14] Furthermore, the inappropriate antibiotic prescription accounts the multidrug-resistant bacteria, which seriously threatens the health of human. Therefore, predictive biomarkers to obtain accurate and early infection diagnosis are essential for timely treatment and the adequate guidance of antibiotic therapy. Procalcitonin (PCT) is considered a specific biomarker in early clinical diagnosis for severe infection diseases and sepsis caused by bacteria, and it is clinically increasingly used for guiding antibiotic therapy.[15,16] PCT is a protein produced by C cells of the thyroid and by the neuroendocrine cells of the lung and the intestine, and it is a peptide precursor of the hormone calcitonin, which is composed of 116 amino acids. The blood level of PCT would rise in response to the proinflammatory stimulus, especially from bacterial sources. Although ≤ 0.1 ng/mL is the normal concentration in healthy patients, a PCT concentration ≥ 0.5 ng/mL is considered positive for the diagnosis of a bacterial infection, and antibiotic therapy is recommended. A concentration over 2 ng/mL implies the occurrence of sepsis. A level of > 10 ng/mL indicates sepsis or septic shock. Hence, new developments for the sensitive, fast, and reliable determination of PCT are still highly important to help the clinicians to make quick and appropriate decisions.

Currently, a wide range of approaches have been developed for determination of PCT, including immunoturbidimetric assay,[17] chemiluminescent immunoassay,[18−25] immunochromatographic assay,[26−31] surface plasmon resonance biosensor,[32−34] electrochemical immunosensor,[35−54] ellipsometry immunosensor,[55] colorimetric immunoassays,[56−58] and fluorescence immunoassay (FIA).[59−64] Although some of them reach impressive sensitivity, these methods present several limitations, such as their high complexity, sophisticated instrumentation requirements, and/or unproven applicability in the real clinical scenario. Neonatal sepsis diagnosis poses a particular challenge because of difficulties in obtaining blood samples or limited volume availability. Therefore, reliable, sensitive, fast, cheaper, self-contained, user friendly, and less

volume-demanding PCT sensing approaches, if developed, could benefit patient outcomes by helping the clinicians in neonatal sepsis diagnostic because it can be an alternative diagnostic tool for onsite/bedside clinical analysis.

In this work, a smartly micromotor-based FIA has been developed for PCT determination as an early biomarker in very low-birth-weight (VLBW) babies with suspected sepsis.

2. Materials and methods

2.1. Reagent and solutions

PCT (8PC5) and two paired monoclonal mouse antihuman PCT antibodies [42 anti-PCT (FITCconjugated) and 16B5 anti-calcitonin (biotinylated)] were obtained from HyTest (Turku, Finland).

Dilution of PCT and antihuman PCT antibodies were prepared in PBS, 0.1 M phosphate (Scharlau, 99%), 0.01% Tween 20 (Sigma-Aldrich), 0.138 M NaCl (Scharlau, 99%), and 2.7 mM KCl (Scharlau, 99%) buffer solution pH 7.5.

Bovine serum albumin (BSA), streptavidin, 1-ethyl-3-(3-dimethylaminopropyl) carbodiimide (EDC), N-hydroxysulfosuccinimide (NHS), and sodium cholate (NaCh) were purchased from Sigma-Aldrich (Madrid, Spain). EDC, NHS, and streptavidin solutions were prepared in MES buffer 0.1 M pH 5. MES monohydrate was obtained from Sigma-Aldrich.

For the micromotor synthesis, the 5 μm-diameter conical pore polycarbonate (PC) membranes were purchased from Whatman (Maidstone, UK). Pyrrole-3-carboxylic acid, EDOT, 3-aminobezoic acid, $NiCl_2 \cdot 6H_2O$, $Ni(H_2NSO_3)_2 \cdot 4H_2O$, and chloroplatinic acid hydrate for micromotor synthesis were obtained from Sigma-Aldrich (Madrid, Spain) and used without further purification.

2.2. Samples

Plasma samples with undetectable PCT concentration (healthy patients) were obtained from anonymous donors with their previous consent.

Hospital Clínico San Carlos (Madrid, Spain) provided unique plasma samples from VLBW (<1500 g) infants. The study was approved by the Ethics Committee

of Hospital Clínico San Carlos, and parental informed consent was obtained before the collection of blood samples. Babies were included in the study only if blood samples were needed as part of the standard care in the neonatal intensive care unit (NICU) and not for the only purpose of the present study.

Samples were obtained by venipuncture. Whole blood (500 µL) was collected in a heparinized tube and transported to the central laboratory of Hospital Clínico San Carlos for standard analysis (BRAHMS PCTsensitive KRYPTOR). Another aliquot of 500 µL of whole blood was collected in a heparinized tube and centrifuged at 1000 rpm for 15 min. The supernatant was separated and transported to the research laboratory on ice. Four different samples were obtained from three NICU patients.

2.3. Apparatus

Template electrochemical deposition of micromotors was carried out using electrochemical station µAutolab Type III (Eco Chemie, Utrecht, Holland). Scanning electron microscopy (SEM) images were obtained with a JEOL JSM 6335F instrument, using an acceleration voltage of 22 kV. Energy-dispersive X-ray mapping analysis was performed using an EDX detector attached to a SEM instrument. An inverted optical microscope (Nikon Eclipse 80i upright microscope), coupled with different objectives (10×, 20×, and 40×), a B2-A fluorescence filter (λ_{ex}, 490 nm; λ_{em}, 520 nm), a Hamamatsu digital camera C11440, and NIS Elements AR 3.2 software, was used for capturing images and movies. The speed of the micromotors was tracked using a NIS Elements tracking module. The fluorescence signals were estimated by analyzing the corresponding time lapse images using the NIS Elements measurement module.

Advanced Vortex Mixer-ZX3 fromVWRand Thermosaker TS-100C from Biosan were used for incubation stages. Magnetic block DynaMag™-2 was obtained from ThermoFisher for the handling of magnetic micromotors.

2.4 Electrochemical synthesis of tubular catalytic micromotors

A set of micromotors differentiated by the polymeric composition of their outer layer were fabricated, according to different protocols, using a PC membrane with 5 µm-diameter conical pores.

The S4-branched side of 5 μm-diameter conical pores of a PC membrane was treated with a sputtered thin gold film to perform as a working electrode. The membrane was assembled in a Teflon-plated cell with aluminum foil serving as an electrical contact to the working electrode for the subsequent electrodeposition. For the synthesis of polymeric outer layer micromotors, electropolymerization of the different conductive monomers [3-aminobenzoic acid (3-ABA), pyrrole-3-carboxylic acid, and EDOT] was carried out. Poly-3-aminobenzoic acid (P3ABA) outer layer was electropolymerized at +0.80 V for 5 s from a plating solution containing 0.1 M 3-ABA, 0.1 M H_2SO_4, and 0.5 M Na_2SO_4 (adapted from ref. 2). The PEDOT/PPy-COOH outer layer was electropolymerized for a total charge of 0.3 C at +0.80 V from a plating solution containing 12 and 3 mM EDOT and pyrrole-COOH monomer in a solution containing 7.5 mM KNO_3 and 100 mM SDS (adapted from ref. 13), respectively. Polypyrrole (PPy) microtubes were electropolymerized at +0.80 V for a charge of 0.15−0.2 C (about 7000 s) from a plating solution containing 25 mM pyrrole-3-carboxylic acid and 7.5 mM KNO_3 (adapted from ref. 2).

All the fabricated micromotors also include a magnetic layer of Ni for their efficient magnetic control and the platinum layer for catalytical propulsion. The nickel tube layer was plated inside the polymeric layer by the galvanostatic method. First, 10 pulses of −20 mA were applied for 0.1 s to generate nucleation spots. Then, a constant current of −6 mA was applied for 300 s to grow the nickel layer. Subsequently, a platinum layer was plated inside the nickel layers. This inner layer, composed of PtNPs, was deposited by amperometry at −0.4 V for 750 s from an aqueous solution containing 4 mM of H_2PtCl_6 in 0.5 M acid boric.

Once the micromotor growth was finished, the sputtered gold layer was gently hand-polished with 1 μm alumina slurry. After this, the membrane was dissolved in methylene chloride for 30 min to completely release the microtubes. The micromotors were placed on the magnet-holding block, and the supernatant was removed. Afterward, successive washes with isopropanol and ethanol (both twice) and ultrapure water (18.2 MΩ.cm, three times) were performed with a 2 min interval on the magnet-holding block between each wash. All microtubes were stored in ultrapure water at room temperature when are not in use. For

control experiments, the micromotors were synthetized following the same protocol, avoiding the electrodeposition of the platinum layer.

2.5. Micromotors functionalization

The set of fabricated micromotors were functionalized in their outer layer with streptavidin in order to immobilize the specific anti-PCT antibody. In this sense, the available carboxyl-terminated groups were activated by the EDC/NHS chemistry. Each time, a stock solution of 800 µL (640 000 microengines approximately) was treated with 200 µL of a 100 mM EDC/NHS solution prepared in 0.1M MES buffer, pH 5.0, and for 30 min at 25 °C. After two washing steps with MES buffer, the activated micromotors were incubated with 200 µL of a 400 µg/mL streptavidin solution in 0.1M MES buffer, pH 5.0, and for 1 h at 25 °C. Two washing steps with MES buffer and an additional washing step with PBS were carried out to eliminate the excess of streptavidin.

Finally, the set of streptavidin-modified micromotors, 25 µL each, were incubated in a solution containing 50 µL of 7.5 µg/mL biotinylated anti-PCT antibody (capture antibody). After room temperature incubation under stirring for 30 min, the tubes were placed on the magnetic-holding block, and the supernatants were removed. Immediately, the supernatants were washed twice with 100 µL of PBS buffer, and the micromotors were resuspended in 25 µL of PBS and maintained at 4 °C.

2.6 Streptavidin immobilization capacity according to the monomeric concentration used for the fabrication of the polypyrrole outer layer in the micromotors

A biotin fluorophore-labeled reagent (Atto 550-biotin) was used in order to evaluate the amount of streptavidin immobilized versus the monomeric concentration used in the fabrication of polypyrrole outer layer in the micromotors. In this sense, three batches containing approximately 20000 micromotors each, and after streptavidin immobilization, were incubated in a 5% BSA blocking solution during 45 min, followed by three washing steps with 100 µL of PBS. Then, each micromotor batch was incubated with 10 µL of biotin fluorophore-labeled reagent in PBS (20 µg/mL) during 15 min. Finally, adequate washing steps were carried out prior to their fluorimetric detection.

2.7 Development of PCT-micromotor immunoassay.

In detail, a solution containing approximately 20 000 micromotors modified with the capture antibody was deposited into a test tube. Then, the sample (25 µL) and detection antibody were added to perform the sandwich immunocomplex in one step. In order to provide the micromotor propulsion, H_2O_2 (2%), which allows the catalytic reaction responsible of the bubble formation in the inner layer of the micromotor, was also deposited into the tube. After 30 min, the micromotor propulsion was stopped by a dilution effect after addition of 200 µL of PBS. Thanks to their magnetic characteristics (intermediate magnetic layer of nickel), micromotors were retained, and the supernatant was removed, followed by three washing steps.

2.8 Fluorescence measurements.

After the immunocomplex formation on board of the micromotors, they were resuspended in 3 µL of PBS solution while 1 µL of this suspension was directly positioned onto a microscope slide to perform the fluorescence measurements at λ_{ex} = 490 nm and λ_{em} = 520 nm. These fluorescence signals were analyzed by the Nikon software associated to the microscope and fitted to the fourparameter logistic equation (**Equation (IV.2.1)**) using the software SigmaPlot 10.0.

$$\mathbf{F}_y = \left(\frac{F_{max} - F_{min}}{1 + \left(\frac{EC_{50}}{x}\right)^h} + F_{min} \right) \quad \text{(IV.2.1)}$$

where F_{max} and F_{min} are the maximum and minimum fluorescence intensity values of the calibration graph, respectively; the EC_{50} value is the analyte concentration corresponding to a 50% of F_{max}; and h is the hill slope. LOD and LOQ were calculated using the 3 S/N and 10 S/N criteria, respectively. S was estimated as sd (n = 10) obtained during the measurement of the current intensity from the lowest CRP concentration used in the calibration, 0.5 ng/mL.

3. Results and discussion

3.1. Micromotor-based immunoassay approach.

As we have stated in the introduction, catalytic self-propelled micromotors have emerged in the last years as highly interesting new tool for biosensing. Actually, their special features, such as their efficient movement into the solution by the generated microbubble tails to find the analyte without the need of external stirring, the induced fluid-mixing effect that enhances the biorecognition event, together with the easiness to functionalize their surface with different bioreceptors, make these micromachines an excellent analytical tool, especially for diagnosis and monitoring in clinical analysis. In this sense, functionalized micromotors were designed for *on-the-move* PCT determination in hardly available plasma samples obtained from VLBWI with suspected sepsis, using minute amounts of samples.

To this end, tubular micromotors were electrosynthetized by concentric layers with precise functions: PPy-COOH-streptavidin outer layer (PPy) as a functionalized support for the specific antibody (anti-PCT) immobilization; a Ni intermediate layer for magnetic guidance; and internal PtNP catalytic layer for the generation of oxygen bubble-mediated propulsion in the presence of H_2O_2 fuel (anti-PCT PPy/Ni/PtNPs) (see **Figure IV.2.1**).

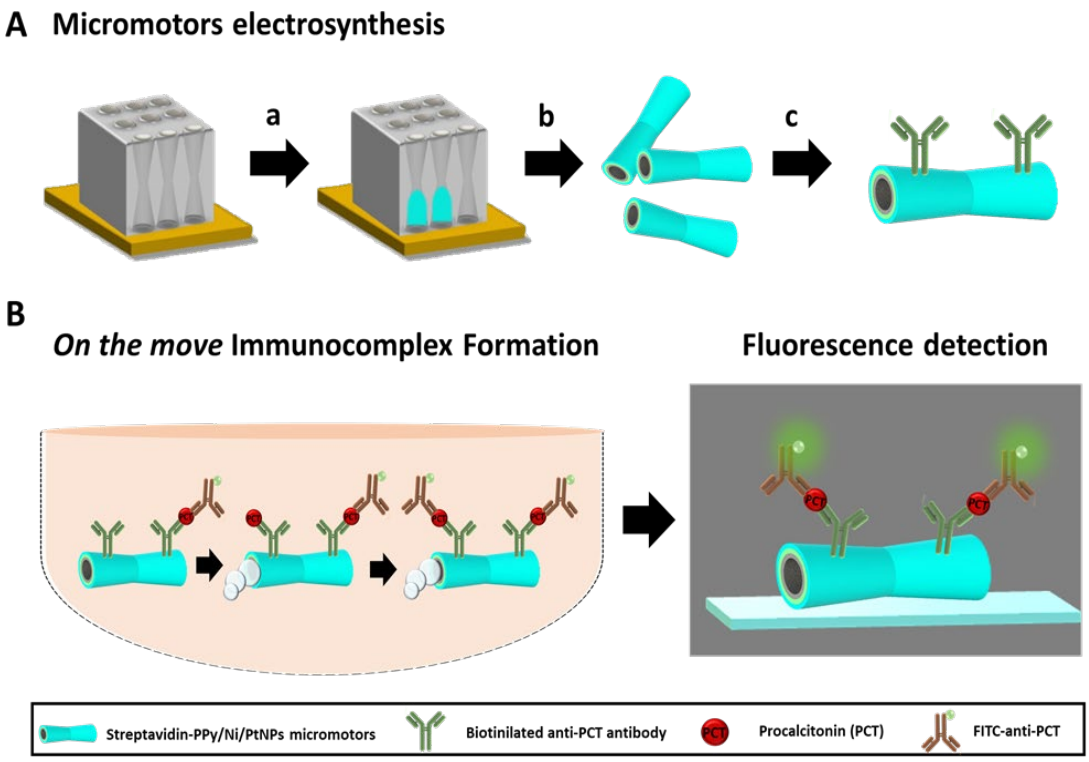

Figure IV.2.1. (A) Schematics of the preparation of anti-PCT-PPy/Ni/PtNPs micromotors: (a) electro polymerization of PPy external layer and sequential electrodeposition of Ni and Pt (medium and inner) layers, (b) removal of the polymeric template (c) micromotors functionalization with streptavidin and biotin-anti-PCT antibodies. (B) Fluorescence micromotor-based immunoassay (FMIm) approach for PCT determination.

The fluorescence micromotor-based immunoassay (FMIm) approach is also depicted in **Figure IV.2.1**. Anti-PCT-functionalized micromotors were added into a cocktail solution that contained the PCT, the anti-PCT detection antibody labeled with a fluorescent dye, and the reagent for propulsion (H_2O_2, 2%). Then, the antibody-functionalized micromotors swim autonomously around the sample to actively bind the specific analyte and the reporter antibody, and the event also improved by the generated microbubble tails and the induced mixing effect. After the immunocomplex formation, the assay was stopped thanks to the dilution effect after addition of PBS and helped by the magnetic properties of the intermedium Ni layer. After the washing step, the supernatant was removed, and the fluorescence detection was carried out on the fluorescence microscope.

3.2 PPy/Ni/PtNP micromotor synthesis and characterization.

The material used in the construction of outer layer is decisive because it influences micromotor antibody immobilization capabilities. Different polymers

containing carboxylic groups have been checked in order to provide the best capture antibody immobilization support. After their functionalization with streptavidin, binding the capture antibody, and developing the immunoassay architecture, **Figure IV.2.2** shows the fluorescence produced by the different polymer-based outer layer micromotors. The PPy micromotors provided the higher signal, which can be attributed to higher amount of exposed carboxylic groups used for binding the specific antibody. Because of its better performance, PPy was chosen as the outer micromotor layer for detecting PCT.

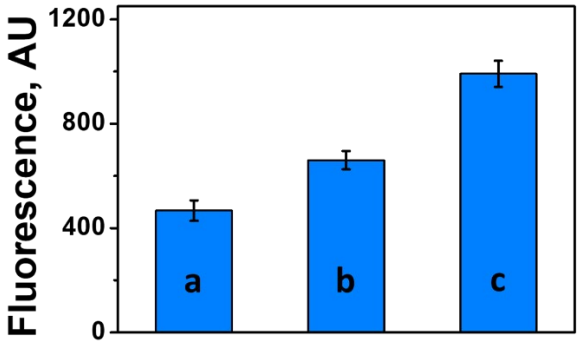

Figure IV.2.2. External layer material selection study, a) PEDOT/PPy-COOH, b) P3ABA, c) PPy-COOH. Immunocomplex formation under stirring conditions (60 min; excess antibodies conditions) ([PCT]=500 ng/mL).

The amount of monomer used on PPy/Ni/PtNP micromotor electrosynthesis had an influence on the micromotor-based immunoassay. Increasing the concentration of the monomer up to 25 mM produced an increment in the fluorescence signal because of accumulative amount of carboxyl groups and, hence, a higher capture antibody immobilization. In addition, SEM images revealed a well-defined conical shape (5 μm width, 20 μm height) and higher micromotor consistence when 25 mM monomer concentration was used for PPy/Ni/PtNP micromotor electrosynthesis, and EDX confirmed the composition of the tailored layers (**Figure IV.2.S1**). Both lower and higher monomer concentrations produced more fragile micromotors that can be partially destroyed during the assay. **Figure IV.2.3** shows this effect when the whole immunoassay architecture was performed and also in a control experiment where the surface-attached streptavidin was evaluated by a biotin-labeled fluorophore.

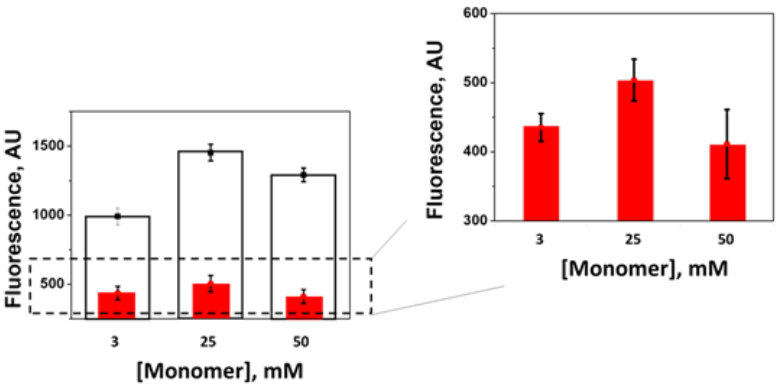

Figure IV.2.3. Influence of the monomer concentration on the binding capacity of polymeric outer layer. In red: streptavidin binding capacity assay. Fluorescence signals due to fluorescence-biotin bound to the streptavidin. In white: Immunosensor fluorescence signals with immunocomplex formation under stirring conditions (60 min). [PCT] = 500 ng/mL.

3.3 Optimization of the PPy/Ni/PtNP micromotor-based immunoassay.

Conceptually, the optimization of the *on-the-move* immunoassay for the determination of PCT includes addressing, not only the variables linked to traditional immunoassay (amount of capture and detection antibodies) but also the variables inherent in the use of catalytic micromotors such as the number of them that allow to reach adequate sensitivity conditions as well as the fuel composition that allows an adequate and efficient propulsion in the clinical media without affecting the analytical behavior of the immunoassay. **Table IV.2.1** summarizes the optimized conditions for the PPy/Ni/PtNP micromotor-based PCT immunoassay.

In principle, the higher amount of micromotors, the higher the signal obtained because larger amount of PCT molecules can be bound to the specific antibodies immobilized onto the micromotors. Nevertheless, an excess of micromotors implies a higher aggregation and a lower effective navigation to bind the analyte. In this sense, this amount was optimized just to have enough binding sites for the highest PCT concentrations in the calibration curve. As can be observed in **Figure IV.2.4A**, the maximum signal is obtained for approximately 20 000 micromotors, reaching a plateau, indicating that the signal is limited by the established PCT concentration. Then, for the fixed amount of micromotors, both the capture and detection antibodies were titrated, being 7.5 and 16 µg/mL the suitable concentrations, respectively.

Table IV.2.1. Optimization of PPy/Ni/PtNP micromotor-based immunoassay for PCT determination.

Parameter	Tested Range	Selected Value
Micromotor number	2000−30000	20 000
Volume of sample, µL	8−50	25
[Streptavidin], µg/mL	200−600	400
[Capture Ab], µg/mL	2.5−30	7.5
[Detection Ab], µg/mL	4−64	16
Block step, [BSA], %	0−7.5	0
Fuel, [H2O2], %	0.5−5	2
Protein + detection Ab incubation time, min	0−60	30

Because of the high sensitivity needed in PCT diagnosis (cut-off 0.5 ng/mL), the volume of sample required was also studied. As can be observed in **Figure IV.2.4B**, 25 µL of sample is the minimum volume required to obtain adequate sensitivity. Even for 1 ng/mL PCT concentration in the sample, almost the maximum signal is reached with this sample volume. A compromise between the sample volume and adequate sensitivity has to be reached.

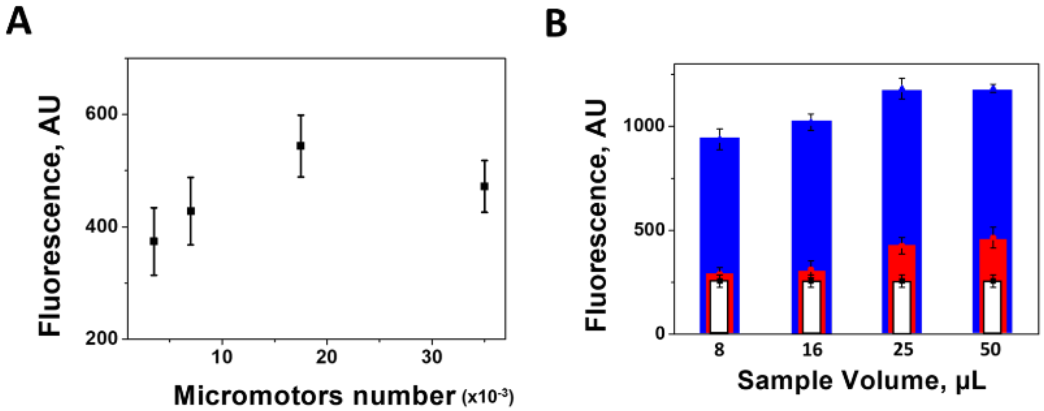

Figure IV.2.4. Optimization of PPy/Ni/PtNPs micromotor-based immunoassay:(A) Influence of the number of PPy/Ni/PtNPs micromotors on the immunoassay (30 min micromotors moving conditions (2% H_2O_2), PCT = 150 ng/mL) and (B) Volume of sample optimization (white bar: 0 ng/mL PCT; red bar: 1 ng/mL blue bar: 1000 ng/mL) (60 min stirring condition).

In contrast with conventional immunosensors, where the analyte interacts with the usually immobilized specific antibody by diffusion or stirring the solution, in

our *on-the-move* immunoassay, self-propelled micromotors actively move around the sample to bind the analyte. The autonomous propulsion of micromotors is produced through the chemical reaction in their platinum inner layer with hydrogen peroxide as the fuel reactant, ejecting oxygen bubbles. The propulsion solution is constituted by hydrogen peroxide, and a surfactant that favors the bubble generation through the interstitial surface tension decreases. H_2O_2 concentration is a crucial parameter because larger concentrations imply too fast movement of micromotors that can produce a bubble excess that restricts the recognition event and/or react with the analyte and the biorecognition element. However, a low fuel concentration reduces the speed of micromotors, slowing down the probability of collisions with the target protein, and avoiding sample homogenization. On the other hand, the surfactant concentration is also a key factor because a high concentration can affect negatively the immunoassay performance by denaturing proteins, breaking protein−protein interactions, and desorbing biomolecules from solid phases.[65] Therefore, a thorough study was addressed to select the suitable concentration of the propulsion components. In order to know the effect of these reagents in the antibody− antigen interaction, a control experiment was performed by the optimized conditions but using micromotors without the platinum intermediate layer under stirring conditions. As can be observed in **Figure IV.2.5A**, an increase in the surfactant concentration produces a decreasing of the fluorescence signal obtained after the whole immunoassay procedure. The remarkable effect at the tested surfactant concentrations can be explained because of the relatively large incubation time needed for immunoreaction (30 min). Surfactant concentration of 1.5% starts to produce the negative effect on the *on-the-move* antigen capture procedure for incubation times longer than 5 min (data not shown). Regarding H_2O_2, **Figure IV.2.5B** shows a significantly negative effect on the immunoassay at higher concentrations than 2% (v/v). In both cases [2% (v/v) H_2O_2−0% NaCh and 1% (v/v) H_2O_2−0.1% (w/v) NaCh], the propulsion performance and speeds of the PPy/Ni/PtNP micromotors (107 ± 30 and 114 ± 20 μm s^{-1}, respectively, see **Video IV.2.S1**) were similar. Consequently, free-surfactant solution [2% (v/v) H_2O_2] was chosen as optimal propulsion condition for subsequent experiments.

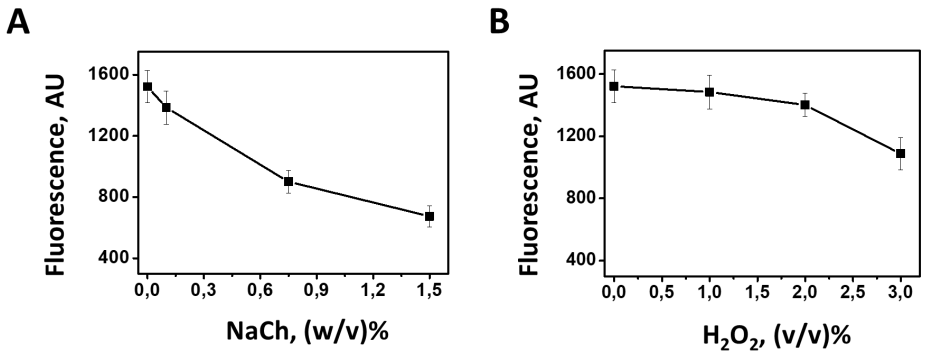

Figure IV.2.5. Effect of the propulsion components on the immunosensor performance: (A) NaCh concentration; (B) H_2O_2 concentration. Experimental conditions: 30 min reaction under stirring conditions, 100 ng/mL PCT.

The time needed to perform the *on-the-move* capture of PCT in the sample was also evaluated. **Figure IV.2.6A** shows the fluorescence signal increment with the *on-the-move* incubation time of up to 30 min. **Figure IV.2.6A** (bottom) shows time lapse images supporting the propulsion of micromotors at different incubation times. The beneficial effect of the *on-the-move* FMIm is confirmed in **Figure IV.2.6B**, where its superior performance is clearly observed in comparison with those obtained in stirring and static conditions.

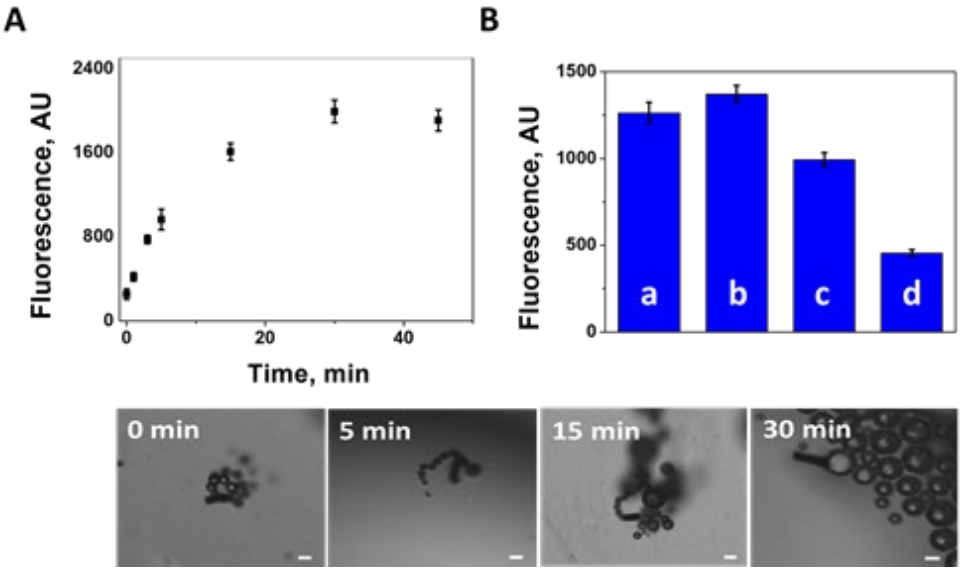

Figure IV.2.6. Optimization for the *on-the-move* immunocomplex formation: (A) Effect of the time on the fluorescence signal (2% (v/v) H_2O_2; 100 ng/mL PCT) and time lapse images of micromotors swimming into plasma samples and (B) Immunoassay performance under different propulsion conditions. (a) 1% (v/v) H_2O_2 – 0.1% (w/v) NaCh. (b) 2% (v/v) H_2O_2 - 0% NaCh. (c) Stirring conditions (950 r.p.m) (d) Static. Experimental conditions: 30 min, 100 ng/mL PCT.

3.4 Analytical performance of micromotor immunoassay and sample analysis

The analytical performance of the anti-PCT-PPy/Ni/PtNP micromotors was carefully studied.

Figure IV.2.7 shows both the sigmoidal and the linear calibration plots obtained for the concentrations assayed, with a wide working linear range between 0.5 and 150 ng/mL. Detection (LOD) and quantification (LOQ) were 0.07 and 0.50 ng/mL, respectively. The LOD and LOQ were calculated using the 3 and 10 S/N criteria, respectively.

Calibration slopes of 550 ± 10 and 539 ± 9 mL ng^{-1} in PBS and plasma samples were obtained, respectively, which indicated the absence of matrix interferences (**Figure IV.2.7B**). At the bottom, optical fluorescence images corresponding to selected PCT concentrations are also depicted, where a fluorescence intensity−PCT concentration dependence is clearly observed (**Figure IV.2.7C**).

Precision was evaluated at two PCT concentration levels (0.5 and 50 ng/mL). The intra-assay precision reached a value of CV = 8% (n = 5) for both concentrations while the inter-assay precision gave CV values of 8 and 9% (n = 5 days) for 0.5 and 50 ng/mL concentrations, respectively.

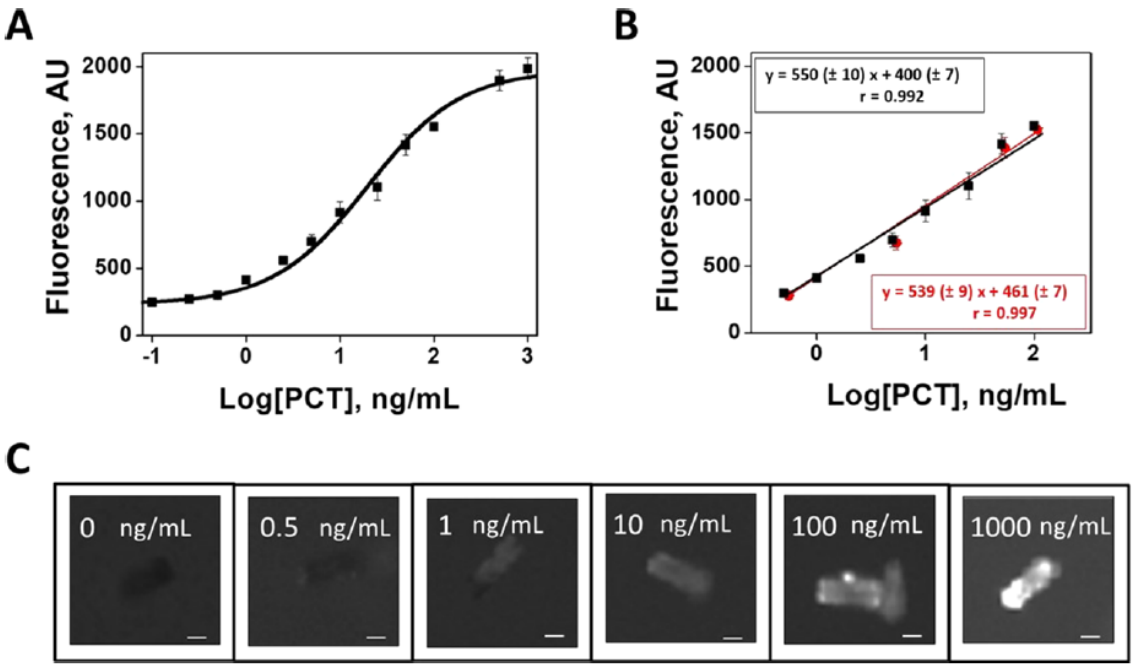

Figure IV.2.7. Calibration of PCT using FMIm approach. (A) Sigmoidal curve of PCT. (B) Linear range of the FMIm (2% H_2O_2, n=3) in buffer and plasma. (C) Fluorescence emission images of different concentrations of PCT. Scale bar: 5 μm.

In order to evaluate the applicability of the developed approach in clinical samples, the micromotor propulsion was also tested in plasma samples. **Video IV.2.S2** illustrates the efficient propulsion of PPy/Ni/PtNP (speed ≈ 90 $\mu m s^{-1}$) and anti-PCT PPy/Ni/PtNP (speed ≈ 70 $\mu m\ s^{-1}$) micromotors in plasma samples under the optimized conditions. As expected, a diminished speed was observed in plasma, although it did not affect the micromotor-sensing capabilities.

Finally, plasma samples from VLBWI with suspected sepsis were analyzed. **Table IV.2.2** lists the sample features and the PCT levels obtained using both, the FMIm approach and the Hospital's method. They revealed a good agreement between the PCT levels obtained by our micromotor-based method and those declared by the Hospital (BRAHMS PCT) ($p < 0.05$). Conceptually speaking and although a direct comparison is not relevant, only magnetic particle-based immunoassays can be reasonably comparable to the magnetic micromotor-based approach proposed in this work and, consequently, only they can be considered as a competitive alternative to such micromotors (see **Table IV.2.S1**).

Table IV.2.2. Analysis of plasma samples of very low birth weight (<1500 g) neonates.[a]

Patient	Sample	$[PCT]_{obtained}$ (ng/mL)	$[PCT]_{hospital}$ (ng/mL)
sex: male, gestational age (weeks): 26^{0}, birth weight (g): 990	1	1.3 ± 0.2	1.5
	2	1.1 ± 0.2	---
sex: male, gestational age (weeks): 30^{3}, birth weight (g): 1400	3	20.4 ± 2.9	21.7
sex: male, gestational age (weeks): 30^{3}, birth weight (g): 1435	4	38.6 ± 5.8	38.9

[a] Results are expressed as mean values ± SD (n=3)

First, our *on-the-fly* biosensing based on magnetic micromotors showed a very good sensitivity with limits of detection (0.07 ng/mL) and quantification (0.5 ng/mL) well enough to determinate the concentration of PCT considered as a threshold (0.5 ng/mL) for a positive diagnosis. Taking into account the importance that PCT has acquired as a biomarker of sepsis, this result is very valuable and promising because, for the first time, the ability of micromotor technology to measure very low PCT concentrations in neonatal clinical samples with sepsis suspicion, which are hardly available, has been evaluated. Only the magnetoimmunoassay reported by Chen *et al*.[26] achieved a lower LOD than the one obtained in our work; however, they used longer analysis times and larger sample volumes (even 40 times higher). In this sense, the works developed by our group [ref. 38, current work] showed shorter analysis times and lower sample volumes, with the exception of the work reported by Qi et al.[25] Nevertheless, this work has not been tested in clinical samples either. Moreover, it can be said that our approach elegantly combined short analysis times using low volumes of clinical samples, which proved to be very suitable for diagnostic purposes using this very unique samples.

In addition, taking into account that there is no need to do external stirring because of their inherent self-propulsion micromotor's capability, which allows agitation in sample microvolumes where conventional agitation cannot be carried out. This characteristic establishes an important difference of (magnetic) micromotors in comparison with other (magnetic) immunoassays for analytical

purposes in low sample volume-based diagnostics. The micromotor-based approach allowed a simplification of the assay, becoming as a real highly competitive alternative to the well-established magnetic bead-based immunoassays as POCT devices.

4. Conclusions

In addition to the key advantages based on sample sizing, FMIm has demonstrated excellent biosensing capabilities for the PCT accurate determination in the whole clinically relevant range, without any dilutions in unique hardly available VLBWI samples with sepsis suspicion.

These results are very revealing because they show the analytical potential of micromotors in the field of biosensing because they have been able to measure the clinically relevant levels of PCT in neonatal sepsis. These results become more important because today there is no doubt that PCT is the most important sepsis protein biomarker. Therefore, micromotors are configured as future tools for early diagnostics (which are essential for timely treatment and the adequate guidance of antibiotic therapy) as well as in the development of *point-of-care* devices.

Acknowledgments

This work was supported by the Spanish Ministry of Economy, Industry and Competitiveness (CTQ2017-86441-C2-1-R), the TRANSNANOAVANSENS program (S2018/NMT-4349) from the Community of Madrid, and La Caixa Impulse program (CI017-00038) (A.E., M.Á.L., M.M.-G., and Á.M.-F.).

Á.M.-F. acknowledges the FPU fellowship from the Spanish Ministry of Education Culture and Sports.

Associated content

Supporting Information

Figure IV.2.S1. SEM images of PPy/Ni/PtNPs prepared under different monomer concentration conditions and EDX analysis of 25mM monomer concentration.

Table IV.2.S1. Analytical characteristics of PCT magneto sandwich immunoassays reported in the literature.

Video IV.2.S1. Propulsion of PPy/Ni/PtNP micromotors using 2% (v/v) H2O2−0% NaCh and 1% (v/v) H_2O_2−0.1% (w/v) NaCh

Video IV2.S2. Efficient propulsion of PPy/Ni/PtNP and anti-PCT PPy/Ni/PtNP micromotor in plasma samples

Authors information

Corresponding authors

Miguel Ángel López − Department of Analytical Chemistry, Physical Chemistry and Chemical Engineering, University of Alcalá, 28871 Alcaláde Henares, Madrid, Spain; Chemical; Research Institute “Andres M. Del Rio”, Universidad de Alcalá, 28871 Alcalá de Henares, Madrid, Spain; Phone: +34 91 885 49 95; Email: miguelan.lopez@uah.es

Alberto Escarpa − Department of Analytical Chemistry, Physical Chemistry and Chemical Engineering, University of Alcalá, 28871 Alcalá de Henares, Madrid, Spain; Chemical Research Institute “Andres M. Del Rio”, Universidad de Alcalá, 28871 Alcalá de Henares, Madrid, Spain; orcid.org/0000-0002-7302-0948; Email: alberto.escarpa@uah.es

Authors

Águeda Molinero-Fernández − Department of Analytical Chemistry, Physical Chemistry and Chemical Engineering, University of Alcalá, 28871 Alcaláde Henares, Madrid, Spain

María Moreno-Guzmán − Department of Chemistry in Pharmaceutical Sciences, Analytical Chemistry, Faculty of Pharmacy, Universidad Complutense de Madrid, 28040 Madrid, Spain

Luis Arruza − Division of Neonatology, Instituto del Niño y del Adolescente, Hospital Clínico San Carlos-IdISSC, 28040 Madrid, Spain

Authors contribution

Á.M.-F. and M.M.-G. contributed equally. The manuscript was written through contributions of all the authors. All the authors have given approval to the final version of the manuscript.

5. References

(1) Guix, M.; Mayorga-Martinez, C. C.; Merkoçi, A. Nano/micromotors in (bio)chemical science applications. *Chem. Rev.* **2014**,*114*, 6285−6322.

(2) Gao, W.; Sattayasamitsathit, S.; Uygun, A.; Pei, A.; Ponedal, A.; Wang, J. Polymer-based tubular microbots: role of composition and preparation. *Nanoscale* **2012**, *4*, 2447−2453.

(3) Fomin, V. M.; Hippler, M.; Magdanz, V.; Soler, L.; Sanchez, S.; Schmidt, O. G. Propulsion Mechanism of Catalytic Microjet Engines. *IEEE Trans. Robot.* **2014**, *30*, 40−48.

(4) Karshalev, E.; Esteban-Fernández de Ávila, B.; Wang, J. Micromotors for “Chemistry-on-the-Fly”. *J. Am. Chem. Soc*. **2018**, *140*, 3810−3820.

(5) Pacheco, M.; López, M. Á.; Jurado-Sánchez, B.; Escarpa, A. Selfpropelled micromachines for analytical sensing: a critical review. *Anal. Bioanal. Chem*. **2019**, *411*, 6561−6573.

(6) Wang, J. Self-propelled affinity biosensors: Moving the receptor around the sample. *Biosens. Bioelectron*. **2016**, *76*, 234−242.

(7) Orozco, J.; Jurado-Sánchez, B.; Wagner, G.; Gao, W.; Vazquez-Duhalt, R.; Sattayasamitsathit, S.; Galarnyk, M.; Cortés, A.; Saintillan, D.; Wang, J. Bubble-Propelled Micromotors for Enhanced Transport of Passive Tracers. *Langmuir* **2014**, *30*, 5082−5087.

(8) Morales-Narváez, E.; Guix, M.; Medina-Sánchez, M.; Mayorga-Martinez, C.; Merkoçi, A. Micromotor Enhanced Microarray Technology for Protein Detection. *Small* **2014**, *10*, 2542−2548.

(9) Kong, L.; Guan, J.; Pumera, M. Micro- and nanorobots based sensing and biosensing. *Curr. Opin. Electrochem*. **2018**, *10*, 174−182.

(10) Gao, W.; Sattayasamitsathit, S.; Orozco, J.; Wang, J. Highly Efficient Catalytic Microengines: Template Electrosynthesis of Polyaniline/Platinum Microtubes. *J. Am. Chem. Soc*. **2011**, *133*, 11862−11864.

(11) Vilela, D.; Orozco, J.; Cheng, G.; Sattayasamitsathit, S.; Galarnyk, M.; Kan, C.; Wang, J.; Escarpa, A. Multiplexed immunoassay based on micromotors and microscale tags. *Lab Chip* **2014**, *14*, 3505−3509.

(12) García, M.; Orozco, J.; Guix, M.; Gao, W.; Sattayasamitsathit, S.; Escarpa, a.; Merkoçi, A.; Wang, J. Micromotor-based lab-on-chip immunoassays. *Nanoscale* **2013**, *5*, 1325−1331.

(13) Orozco, J.; Pan, G.; Sattayasamitsathit, S.; Galarnyk, M.; Wang, J. Micromotors to capture and destroy anthrax simulant spores. *Analyst* **2015**, *140*, 1421−1427.

(14) World Health Organization. *World Health Statistics*, **2019**.

(15) Vijayan, A. L.; Vanimaya; Ravindran, S.; Saikant, R.; Kartik, R.; Manoj, G. Procalcitonin: a promising diagnostic marker for sepsis and antibiotic therapy. *J. Intensive Care* **2017**, *5*, 51.

(16) Meisner, M. Update on procalcitonin measurements. *Ann. Lab. Med.* **2014**, *34*, 263−273.

(17) Dipalo, M.; Guido, L.; Micca, G.; Pittalis, S.; Locatelli, M.; Motta, A.; Bianchi, V.; Callegari, T.; Aloe, R.; Da Rin, G.; Lippi, G. Multicenter comparison of automated procalcitonin immunoassays. *Pract. Lab. Med*. **2015**, *2*, 22−28.

(18) Xue, J.; Yang, L.; Jia, Y.; Wang, H.; Zhang, N.; Ren, X.; Ma, H.; Wei, Q.; Ju, H. Electrochemiluminescence Double Quenching System Based on Novel Emitter $GdPO_4$:Eu with Low-Excited Positive Potential for Ultrasensitive Procalcitonin Detection. *ACS Sens*. **2019**, *4*, 2825−2831.

(19) Chen, P.; Xia, F.; Tian, D.; Zhou, C. A Dual-Coreactants Electrochemiluminescent Immunosensor for Procalcitonin Detection Based on CdS-MoS_2 Nanocomposites. *J. Electrochem. Soc*. **2018**, *165*, B196−B201.

(20) Jia, Y.; Yang, L.; Xue, J.; Zhang, N.; Fan, D.; Ma, H.; Ren, X.; Hu, L.; Wei, Q. Bioactivity-Protected Electrochemiluminescence Biosensor Using Gold Nanoclusters as the Low-Potential Luminophor and Cu_2S Snowflake as Co-reaction Accelerator for Procalcitonin Analysis. *ACS Sens*. **2019**, *4*, 1909−1916.

(21) Chen, P.; Qiao, X.; Liu, J.; Xia, F.; Tian, D.; Zhou, C. A dual signals response electrochemiluminescence immunosensor based on PTC-DEPA/KCC-1 NCs for detection of procalcitonin. *Sens. Actuators, B* **2018**, *267*, 525−532.

(22) Xu, X.; Song, X.; Nie, R.; Yang, Y.; Chen, Y.; Yang, L. Ultrasensitive capillary immunosensor combining porous-layer surface modification and biotin-streptavidin nano-complex signal amplification: Application for sensing of procalcitonin in serum. *Talanta* **2019**, *205*, 120089.

(23) Li, H.; Sun, Y.; Elseviers, J.; Muyldermans, S.; Liu, S.; Wan, Y. A nanobody-based electrochemiluminescent immunosensor for sensitive detection of human procalcitonin. *Analyst* **2014**, *139*, 3718−3721.

(24) Tian, Y.; Lv, J.; Wang, J.; Qin, Y.; Liu, J.; Zhao, W. A light initiated chemiluminescent immunoassay for procalcitonin. *Acta Biochim. Biophys. Sin.* **2014**, *46*, 817−819.

(25) Qi, S.; Li, Q.; Rao, W.; Liu, X.; Yin, L.; Zhang, H. Determining the concentration of procalcitonin using a magnetic particles-based chemiluminescence assay for the clinical diagnosis of sepsis. *Anal. Sci*. **2013**, *29*, 805−810.

(26) Chen, Y.; Xianyu, Y.; Wu, J.; Dong, M.; Zheng, W.; Sun, J.; Jiang, X. Double-enzymes-mediated bioluminescent sensor for quantitative and ultrasensitive point-of-care testing. *Anal. Chem*. **2017**, *89*, 5422−5427.

(27) Taranova, N. A.; Urusov, A. E.; Sadykhov, E. G.; Zherdev, A. V.; Dzantiev, B. B. Bifunctional gold nanoparticles as an agglomerationenhancing tool for highly sensitive lateral flow tests: a case study with procalcitonin. *Microchim. Acta* **2017**, *184*, 4189−4195.

(28) Wang, H.; Wang, H.; Chen, S.; Dzakah, E. E.; Kang, K.; Wang, J.; Wang, J. Development of a fluorescent immnunochromatographic assay for the procalcitonin detection of clinical patients in China. *Clin. Chim. Acta* **2015**, *444*, 37−42.

(29) Zhao, Y.; Zhou, C.; Wu, R.; Li, L.; Shen, H.; Li, L. S. Preparation of multi-shell structured fluorescent composite nanoparticles for ultrasensitive human procalcitonin detection. *RSC Adv*. **2015**, *5*, 5988−5995.

(30) Tang, J.; Lei, L.; Feng, H.; Zhang, H.; Han, Y. Preparation of K+-Doped Core-Shell NaYF4:Yb, Er Up conversion Nanoparticles and its Application for

Fluorescence Immunochromatographic Assay of Human Procalcitonin. *J. Fluoresc.* **2016**, *26*, 2237.

(31) Xu, X.; Song, X.; Nie, R.; Yang, Y.; Chen, Y.; Yang, L. Ultrasensitive capillary immunosensor combining porous-layer surface modification and biotin-streptavidin nano-complex signal amplification: Application for sensing of procalcitonin in serum. *Talanta* **2019**, *205*, 120089.

(32) Nie, R.; Xu, X.; Cui, X.; Chen, Y.; Yang, L. A Highly Sensitive Capillary-Based Immunosensor by Combining with Peroxidase Nanocomplex- Mediated Signal Amplification for Detection of Procalcitonin in Human Serum. *ACS Omega* **2019**, *4*, 6210−6217.

(33) Vashist, S. K.; Schneider, E. M.; Barth, E.; Luong, J. H. T. Surface plasmon resonance-based immunoassay for procalcitonin. *Anal. Chim. Acta* **2016**, *938*, 129−136.

(34) Jing, W.; Wang, Y.; Yang, Y.; Wang, Y.; Ma, G.; Wang, S.; Tao, N. Time-Resolved Digital Immunoassay for Rapid and Sensitive Quantitation of Procalcitonin with Plasmonic Imaging. *ACS Nano* **2019**, *13*, 8609−8617.

(35) Sener, G.; Ozgur, E.; Rad, A. Y.; Uzun, L.; Say, R.; Denizli, A. Rapid real-time detection of procalcitonin using a microcontact imprinted surface plasmon resonance biosensor. *Analyst* **2013**, *138*, 6422−6428.

(36) Yang, Z.-H.; Ren, S.; Zhuo, Y.; Yuan, R.; Chai, Y.-Q. Cu/Mn Double-Doped CeO_2 Nanocomposites as Signal Tags and Signal Amplifiers for Sensitive Electrochemical Detection of Procalcitonin. *Anal. Chem*. **2017**, *89*, 13349−13356.

(37) Chiang, C.Y.; Huang, T.T.; Wang, C.H.; Huang, CJ.; Tsai, T.H.; Yu, S.N.; Chen, Y.T.; Hong, S.W.; Hsu, C.W.; Chang, T.C.; Chau, L.K. Fiber optic nanogold-linked immunosorbent assay for rapid detection of procalcitonin at femtomolar concentration level. *Biosens. Bioelectron*. **2019**, *151*, 111871.

(38) Molinero-Fernández, Á.; Moreno-Guzmán, M.; Arruza, L.; López, M. Á.; Escarpa, A. Toward Early Diagnosis of Late-Onset Sepsis in Preterm Neonates: Dual Magnetoimmunosensor for Simultaneous Procalcitonin and C-Reactive Protein Determination in Diagnosed Clinical Samples. *ACS Sens.* **2019**, *4*, 2117−2123.

(39) Lim, J. M.; Ryu, M. Y.; Kim, J. H.; Cho, C. H.; Park, T. J.; Park, J. P. An electrochemical biosensor for detection of the sepsis-related biomarker procalcitonin. *RSC Adv*. **2017**, *7*, 36562−36565.

(40) Fang, Y.; Hu, Q.; Yu, X.; Wang, L. Ultrasensitive electrochemical immunosensor for procalcitonin with signal enhancement based on zinc nanoparticles functionalized ordered mesoporous carbon-silica nanocomposites. *Sens. Actuators, B* **2018**, *258*, 238−245.

(41) Seshadri, P.; Manoli, K.; Schneiderhan-Marra, N.; Anthes, U.; Wierzchowiec, P.; Bonrad, K.; Di Franco, C.; Torsi, L. Low-picomolar, label-free procalcitonin

analytical detection with an electrolyte-gated organic field-effect transistor based electronic immunosensor. *Biosens. Bioelectron.* **2018**, *104*, 113−119.

(42) Liu, A.; Wang, X. Amperometric Immunosensor of Procalcitonin Based on Amplification Strategy of Ferrocene-Modified Gold nanoparticles. *Int. J. Electrochem. Sci.* **2015**, *10*, 9342−9350.

(43) Sui, Y.; Xu, A.; Jin, X.; Zheng, J.; He, X.; Cheng, Y.; Xie, Q.; Liu, R. In situ enzymatic generation of gold for ultrasensitive amperometric sandwich immunoassay of procalcitonin. *Biosens. Bioelectron*. **2018**, *117*, 422−428.

(44) Zhang, T.; Ren, X.; Fan, D.; Kuang, X.; Wang, H.; Wu, D.; Wei, Q. Electrochemical procalcitonin immunoassay based on Au@Ag heterojunction nanorods as labels and CeO_2-CuO nanorods as enhancer. *Sens. Actuators, B* **2019**, *297*, 126800.

(45) Gao, Z.; Li, Y.; Zhang, C.; Zhang, S.; Jia, Y.; Dong, Y. An enzymefree immunosensor for sensitive determination of procalcitonin using NiFe PBA nanocubes@TB as the sensing matrix. *Anal. Chim. Acta* **2020**, *1097*, 169.

(46) Ghrera, A. S. Quantum dot modified interface for electrochemical immunosensing of procalcitonin for the detection of urinary tract infection. *Anal. Chim. Acta* **2019**, *1056*, 26−33.

(47) Qian, Y.; Feng, J.; Wang, H.; Fan, D.; Jiang, N.; Wei, Q.; Ju, H. Sandwich-type signal-off photoelectrochemical immunosensor based on dual suppression effect of PbS quantum dots/Co_3O_4 polyhedron as signal amplification for procalcitonin detection. *Sens. Actuators, B* **2019**, *300*, 127001.

(48) Mahe, L. S. A.; Green, S. J.; Winlove, C. P.; Jenkins, A. T. A. Pyrene-wired antibodies on highly oriented pyrolytic graphite as a labelfree impedance biosensor for the sepsis biomarker procalcitonin. *J. Solid State Electrochem*. **2014**, *18*, 3245−3249.

(49) Shen, W.-J.; Zhuo, Y.; Chai, Y.-Q.; Yang, Z.-H.; Han, J.; Yuan, R. Enzyme-free electrochemical Immunosensor based on host−guest Nanonets catalyzing amplification for Procalcitonin detection. *ACS Appl. Mater. Interfaces* **2015**, *7*, 4127−4134.

(50) Yang, Z.-H.; Zhuo, Y.; Yuan, R.; Chai, Y.-Q. Electrochemical activity and electrocatalytic property of cobalt phthalocyanine nanoparticles- based immunosensor for sensitive detection of procalcitonin. *Sens. Actuators, B* **2016**, *227*, 212−219.

(51) Liu, F.; Xiang, G.; Yuan, R.; Chen, X.; Luo, F.; Jiang, D.; Huang, S.; Li, Y.; Pu, X. Procalcitonin sensitive detection based on graphene−gold nanocomposite film sensor platform and single-walled carbon nanohorns/hollow Pt chains complex as signal tags. *Biosens. Bioelectron*. **2014**, *60*, 210−217.

(52) Liu, F.; Xiang, G.; Chen, X.; Luo, F.; Jiang, D.; Huang, S.; Li, Y.; Pu, X. A novel strategy of procalcitonin detection based on multinanomaterials of single-

walled carbon nanohorns−hollow Pt nanospheres/ PAMAM as signal tags. *RSC Adv*. **2014**, *4*, 13934−13940.

(53) Fang, Y.-S.; Wang, H.-Y.; Wang, L.-S.; Wang, J.-F. Electrochemical immunoassay for procalcitonin antigen detection based on signal amplification strategy of multiple nanocomposites. *Biosens. Bioelectron*. **2014**, *51*, 310−316.

(54) Li, P.; Zhang, W.; Zhou, X.; Zhang, L. C60 carboxyfullerenebased functionalised nanohybrids as signal-amplifying tags for the ultrasensitive electrochemical detection of procalcitonin. *Clin. Biochem*. **2015**, *48*, 156−161.

(55) Li, Y.; Liu, W.; Jin, G.; Niu, Y.; Chen, Y.; Xie, M. Label-free sandwich imaging ellipsometry immunosensor for serological detection of procalcitonin. *Anal. Chem.* **2018**, *90*, 8002−8010.

(56) Kremmer, E.; Meyer, K.; Grässer, F. A.; Flatley, A.; Kösters, M.; Luppa, P. B.; Krämer, P. M. A new strategy for the development of monoclonal antibodies for the determination of human procalcitonin in serum samples. *Anal. Bioanal. Chem*. **2012**, *402*, 989−995.

(57) Zhang, Y.; Si, X.; Zhang, M.; Yang, X.; Yuan, H.; Wang, X.; Zhang, Y.; Wang, H. Rapid Colorimetric Determination of Procalcitonin Using Magnetic Separation and Enzymatic Catalysis. *Anal. Lett.* **2019**, *52*, 602−612.

(58) Liao, T.; Yuan, F.; Yu, H.; Li, Z. An ultrasensitive ELISA method for the detection of procalcitonin based on magnetic beads and enzymeantibody labeled gold nanoparticles. *Anal. Methods* **2016**, *8*, 1577−1585.

(59) Baldini, F.; Bolzoni, L.; Giannetti, A.; Kess, M.; Krämer, P. M.; Kremmer, E.; Porro, G.; Senesi, F.; Trono, C. A new procalcitonin optical immunosensor for POCT applications. *Anal. Bioanal. Chem*. **2009**, *393*, 1183−1190.

(60) Buchegger, P.; Preininger, C. Four Assay Designs and On-Chip Calibration: Gadgets for a Sepsis Protein Array. *Anal. Chem*. **2014**, *86*, 3174−3180.

(61) Kemmler, M.; Sauer, U.; Schleicher, E.; Preininger, C.; Brandenburg, A. Biochip point-of-care device for sepsis diagnostics. *Sens. Actuators, B* **2014**, *192*, 205−215.

(62) Krämer, P. M.; Kess, M.; Kremmer, E.; Schulte-Hostede, S. Multi-parameter determination of TNFα, PCT and CRP for point-ofcare testing. *Analyst* **2011**, *136*, 692−695.

(63) Rascher, D.; Geerlof, A.; Kremmer, E.; Krämer, P.; Schmid, M.; Hartmann, A.; Rieger, M. Total internal reflection (TIRF)-based quantification of procalcitonin for sepsis diagnosis − A point-of-care testing application. *Biosens. Bioelectron*. **2014**, *59*, 251−258.

(64) Sauer, U.; Domnanich, P.; Preininger, C. Protein chip for the parallel quantification of high and low abundant biomarkers for sepsis. *Anal. Biochem*. **2011**, *419*, 46−52.

(65) Otzen, D. Protein-surfactant interactions: a tale of many states. *Biochim. Biophys. Acta* **2011**, *1814*, 562−591.

Supporting Information

Supporting Figures:

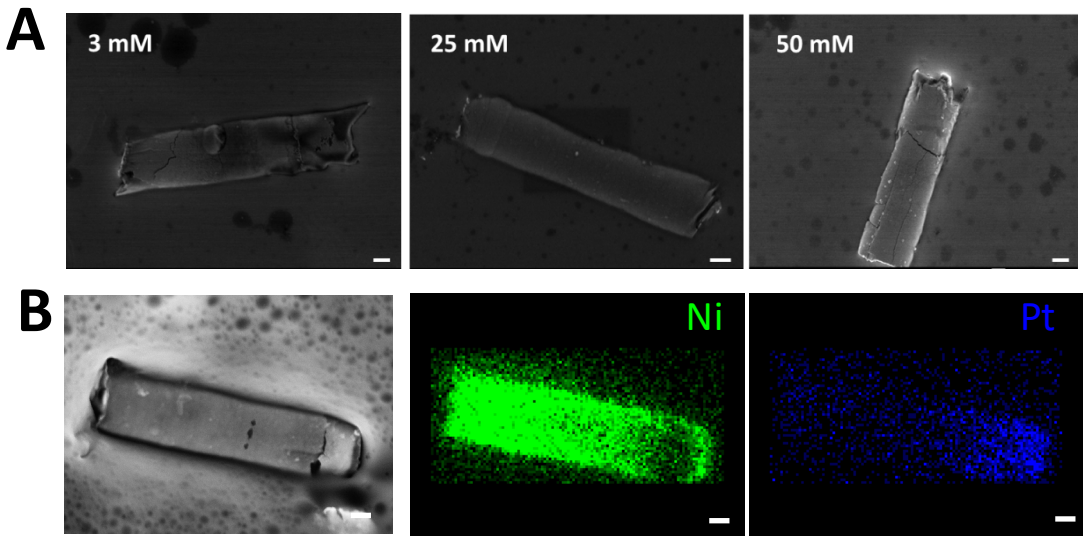

Figure IV.2.S1. (A) SEM images of PPy/Ni/PtNPs prepared under different monomer concentration conditions. (B) EDX analysis of 25mM monomer concentration. Scale bar: 1µm.

Supporting Tables:

Table IV.2.S1. Analytical characteristics of PCT magneto sandwich immunoassays reported in the literature.

Detection	LOD	Time	Sample	Sample Volume	Ref.
Chemiluminiscence	30 pg/mL	25 min	Serum sample diluted	40 µL	25
Chemiluminiscence	0.045 pg/mL	1 h	Clinical Serum	800 µL	26
UV-vis Spectroscopy	40 pg/mL	1 .5 h	Commercial Serum	100 µL	57
UV-vis Spectroscopy	20 pg/mL	1.5 h	Clinical Serum	50 µL	58
Amperometry	50 pg/mL	20 min	Clinical Plasma from neonates	25 µL	38
Fluorescence	70 pg/mL	30 min	Clinical Plasma from neonates	25µL	Our work

Supporting Videos:

Video IV.2.S1. showing propulsion of PPy/Ni/PtNPs micromotors using 2% (v/v) H_2O_2 - 0% NaCh and 1% (v/v) H_2O_2 – 0.1% (w/v) NaCh.

Video IV.2.S2. illustrates the efficient propulsion of PPy/Ni/PtNPs and anti-PCT PPy/Ni/ PtNPs micromotor in plasma samples.